Systems/Circuits

Tunable Action Potential Repolarization Governed by Kv3.4 Channels in Dorsal Root Ganglion Neurons

Tyler D. Alexander,[1,2,4*] Tanziyah Muqeem,[1,2,4*] Lianteng Zhi,[1,2,4] Stephen R. Tymanskyj,[1,2,3,4] and Manuel Covarrubias[1,2,3,4]

[1]Department of Neuroscience, Thomas Jefferson University, Philadelphia, Pennsylvania 19107, [2]Vicki & Jack Farber Institute of Neuroscience at Jefferson Health, Philadelphia, Pennsylvania 19107, [3]Jefferson Synaptic Biology Center, Thomas Jefferson University, Philadelphia, Pennsylvania 19107, and [4]Sidney Kimmel Medical College, Thomas Jefferson University, Philadelphia, Pennsylvania 19107

The Kv3.4 channel regulates action potential (AP) repolarization in nociceptors and excitatory synaptic transmission in the spinal cord. We hypothesize that this is a tunable role governed by protein kinase-C-dependent phosphorylation of the Kv3.4 cytoplasmic N-terminal inactivation domain (NTID) at four nonequivalent sites. However, there is a paucity of causation evidence linking the phosphorylation status of Kv3.4 to the properties of the AP. To establish this link, we used adeno-associated viral vectors to specifically manipulate the expression and the effective phosphorylation status of Kv3.4 in cultured dorsal root ganglion (DRG) neurons from mixed-sex rat embryos at embryonic day 18. These vectors encoded GFP (background control), wild-type (WT) Kv3.4, phosphonull (PN) Kv3.4 mutant (PN = S[8,9,15,21]A), phosphomimic (PM) Kv3.4 mutant (PM = S[8,9,15,21]D), and a Kv3.4 nonconducting dominant-negative (DN) pore mutant (DN = W429F). Following viral infection of the DRG neurons, we evaluated transduction efficiency and Kv3.4 expression and function via fluorescence microscopy and patch clamping. All functional Kv3.4 constructs induced current overexpression with similar voltage dependence of activation. However, whereas Kv3.4-WT and Kv3.4-PN induced fast transient currents, the Kv3.4-PM induced currents exhibiting impaired inactivation. In contrast, the Kv3.4-DN abolished the endogenous Kv3.4 current. Consequently, Kv3.4-DN and Kv3.4-PM produced APs with the longest and shortest durations, respectively, whereas Kv3.4-WT and Kv3.4-PN produced intermediate results. Moreover, the AP widths and maximum rates of AP repolarization from these groups are negatively correlated. We conclude that the expression and effective phosphorylation status of the Kv3.4 NTID confer a tunable mechanism of AP repolarization, which may provide exquisite regulation of pain signaling in DRG neurons.

Key words: **action potential plasticity; Kv channel phosphorylation; Kv3.4 inactivation; nociception**

Significance Statement

The AP is an all-or-none millisecond-long electrical impulse that encodes information in the frequency and patterns of repetitive firing. However, signaling may also depend on the plasticity and diversity of the AP waveform. For instance, the shape and duration of the AP may regulate nociceptive synaptic transmission between a primary sensory afferent to a secondary neuron in the spinal cord. Here, we used mutants of the Kv3.4 voltage-gated potassium channel to manipulate its expression and effective phosphorylation status in dorsal root ganglion neurons and directly show how the expression and malleable inactivation properties of Kv3.4 govern the AP duration and repolarization rate. These results elucidate a mechanism of neural AP plasticity that may regulate pain signaling.

Received June 20, 2022; revised Sep. 1, 2022; accepted Sep. 27, 2022.

Author contributions: T.D.A., T.M., L.Z., and M.C. designed research; T.D.A., T.M., L.Z., and S.R.T. performed research; T.M., L.Z., and M.C. analyzed data; T.D.A., T.M., L.Z., and M.C. wrote the paper.

T. Muqeem's present address: Department of Neurology, Duke University Hospital, Durham, North Carolina 27703.

M.C. was supported by Autifony Therapeutics, the Farber Discovery Fund, and the Jefferson Synaptic Biology Center. T.D.A. and T.M. were supported by the Dubbs Fellowship Fund. We thank Drs. David M. Ritter and Benjamin Zemel for feedback on an earlier version of the manuscript and Dr. Maria Yolanda Covarrubias for fluorescence imaging assistance.

*T.D.A. and T.M. are co-first authors.

The authors declare no competing financial interests.

Correspondence should be addressed to Manuel Covarrubias at Manuel.Covarrubias@jefferson.edu.

https://doi.org/10.1523/JNEUROSCI.1210-22.2022

Introduction

The action potential (AP) in the nervous system is a fast all-or-none electrical event that propagates along axons to allow effective communication over long distances (Bean, 2007). Diverse trains of APs carry relevant information in their frequency of repetitive firing and the patterns of firing (Bean, 2007). However, individual APs are also diverse and plastic and may convey relevant information in their shape and duration, which is often determined by voltage-gated K^+ (Kv) channels (Hochner and Kandel, 1992; Quattrocki et al., 1994; Ma and Koester, 1996; Koch, 1999; Mitterdorfer and Bean, 2002; Carter and Bean, 2009;

Liu and Bean, 2014; Kimm et al., 2015; Pathak et al., 2016; Liu et al., 2017; Zheng et al., 2019). At the synaptic level, these properties may have an impact on evoked synaptic transmission and thereby regulate synaptic strength (Rowan et al., 2014, 2016; Rowan and Christie, 2017; Muqeem et al., 2018; Zemel et al., 2018). Here, we demonstrate how the Kv3.4 channel and its dramatic modulation by protein kinase C (PKC) are directly implicated in tuning AP repolarization in dorsal root ganglion (DRG) neurons.

The Kv3 subfamily includes four high-voltage-activating K^+ channels, Kv3.1, Kv3.2, Kv3.3, and Kv3.4 (Rudy and McBain, 2001; Kaczmarek and Zhang, 2017). Whereas Kv3.1 and Kv3.2 typically induce slow/noninactivating outward currents, Kv3.3 and Kv3.4 induce inactivating outward currents under basal conditions (Kaczmarek and Zhang, 2017). However, macroscopic Kv3.4 currents exhibit the fastest rate of inactivation, which is dramatically slowed upon PKC phosphorylation of the cytoplasmic N-terminal inactivation domain (NTID) of the channel at four sites (S8, S9, S15, and S21; Rudy et al., 1991; Schröter et al., 1991; Covarrubias et al., 1994; Beck et al., 1998; Antz et al., 1999). Kv3.3 exhibits similar modulation, albeit that it involves two sites only (Desai et al., 2008). Previously, we showed that PKC-dependent elimination of fast Kv3.4 N-type inactivation involves a conformational shift of the NTID from compact folding to disordered and that phosphorylation at S8 and S9 is particularly effective at inducing this shift (Beck et al., 1998; Antz et al., 1999). Moreover, to demonstrate that electrostatic interactions underlie the modulation of Kv3.4 inactivation by NTID phosphorylation, we showed that phosphomimetic aspartate mutations of the relevant NTID serine residues closely recapitulate the effects of PKC activation either individually or combined (S[8,9,15,21]D; Beck et al., 1998). By contrast, the phosphonull (PN) Kv3.4 construct in which all relevant serines are mutated to alanine (S[8,9,15,21]A) exhibits no elimination of N-type inactivation upon PKC activation (Covarrubias et al., 1994; Beck et al., 1998). Demonstrating the potential significance of the modulation of fast Kv3.4 inactivation by PKC in a native neural system, we also found that PKC activation in small-diameter DRG neurons eliminates fast inactivation of Kv3.4 and that this is correlated with shortened APs and an accelerated maximum rate of repolarization (Ritter et al., 2012). Critically, this modulation was eliminated when Kv3.4 was knocked down, which prolongs the AP by itself (Ritter et al., 2012). These studies strongly suggest that Kv3.4 is a major regulator of AP repolarization and implicate its modulation by PKC-dependent phosphorylation in this role. However, a direct causal link between the effective phosphorylation status of the Kv3.4 NTID, current kinetics, and the repolarization rate and duration of APs in a neural system is lacking. Addressing this problem is significant because the studies mentioned above mainly relied on the effects of PKC activation by phorbol esters and receptor agonists, which can also modulate other ion channels directly or through other downstream signaling cascades that modulate the AP. To bridge this critical gap in knowledge and establish the causal mechanism of the modulation in a neural setting, we created several adeno-associated-viral (AAV) vectors encoding constructs that specifically manipulate the expression, function, and modulation of Kv3.4 in cultured rat embryonic DRG neurons. Following transduction and analysis of expression and function under voltage- and current-clamping conditions, the results demonstrate a tunable AP repolarization rate and duration that depends on the expression and effective phosphorylation of the Kv3.4 NTID at four sites.

Materials and Methods

Reagents. The rat Kv3.4 cDNA was a gift from Olaf Pongs (University of Hamburg, Germany). Phosphomimic (PM) mutation (S8D, S9D, S15D, S21D), phosphonull (PN) mutation (S8A, S9A, S15A, S21A), and dominant negative (DN) mutation (W429F) were generated through QuikChange mutagenesis based on the rKv3.4WT sequence. The wild-type and mutants were spliced into an AAV backbone vector including the hSyn promoter to drive transcription and the IRES element to allow bicistronic expression of the Kv3.4 gene and GFP. AAV6 packaging was done at the Duke Viral Vector Core facility (Duke University), which provided genomic titers $>10^{12}$ particles/ml (*in vivo* grade).

Dissociation and culturing of embryonic DRG neurons. All animals were treated according to protocols approved by the Institutional Animal Care and Use Committee of Thomas Jefferson University. Time-pregnant female Sprague Dawley rats, embryonic day (E)18, were obtained from Taconic Farms. Embryos from both sexes were dissected in Leibovitz's L-15 medium after the female was killed by overdose of ketamine (380 mg/kg), xylazine (40 mg/kg), and acepromazine (0.3 mg/kg). The process for harvesting and culturing the DRG neurons was as previously described (Tymanskyj et al., 2022). Briefly, DRGs were harvested from all accessible levels and placed into Hanks' buffered saline solution (HBSS) with 10 mM HEPES, followed by two washes with HBSS. After incubation at 37°C with 0.25% trypsin for 10–15 min, the tissue was resuspended in L-15 medium plus 10% horse serum and then mechanically triturated with a fire-polished glass pipette. Dissociated rat DRG neurons were then plated on 18 mm glass coverslips coated with polyornithine and 10 μg/ml laminin in F12 medium (with the N3 supplement, 40 mM glucose, and 25 ng/ml NGF). The following day, the cultured DRG neurons were exposed to $\sim 10^9$ viral genomes of AAV6 vectors containing the Kv3.4 expression constructs described above, as well as the GFP-only expression construct. The media was exchanged two to three times over the next 4–9 d postinfection, and the coverslips with DRG neurons from the different groups were used for immunohistochemical and/or electrophysiological analyses starting on day 6 postinfection.

Immunohistochemistry. DRG neurons not used for electrophysiology were fixed with 4% PFA for 10 min and subsequently blocked with PBS containing 0.2% Triton X-100 and 10% goat serum for 1 h at room temperature. Coverslips were then stained overnight at 4°C in PBS containing 0.2% Triton X-100, 10% goat serum, and rabbit anti-Kv3.4 antibody (1:1000, Alomone Labs). After washing three times with PBS containing 0.2% Triton X-100 for 5 min, coverslips were incubated 30 min at room temperature with goat anti-rabbit Alexa Fluor 594 (1:1000, Invitrogen) in PBS containing 0.2% Triton X-100, and 10% goat serum. Coverslips were then washed with PBS and mounted on a slide using DAPI Prolong Gold Antifade Reagent. Images were taken with a Nikon A1R microscope at the Bioimaging Facility of the Sidney Kimmel Cancer Center of Thomas Jefferson University.

Patch-clamp electrophysiology. Patch-clamping electrodes were made from Corning 7056 thin-wall capillary glass (Warner Instruments) and pulled with a P-97 micropipette puller (Sutter Instruments). Electrodes were fire polished to have tip resistances of 1–3.5 MΩ. Signals were amplified using a MultiClamp 700B amplifier (Molecular Devices), low-pass filtered at 2 kHz (four-pole Bessel), digitized at 10 kHz (Digidata 1440, Molecular Devices), and stored in a computer using Clampex 10.2 software (Molecular Devices). In cell-attached macropatch experiments on infected DRG neurons, the bath and pipette solution contained the following (in mM): 130 choline-Cl, 5 KCl, 1 $MgCl_2$, 2 $CaCl_2$, 10 HEPES, and 50 sucrose, pH 7.4, adjusted with choline base. The membrane potential in the cell-attached configuration was estimated from the following relation: $V_M = V_C - V_R$, where V_C is the command voltage and V_R is the resting membrane potential of the neurons. In agreement with experimental measurements, V_R was assumed to be −60 mV (global mean, -60.26 ± 0.72 mV, $n = 111$ neurons; see Table 2). The voltage protocol shown (see Fig. 2*F*) was used to generate peak current–voltage relations. The conditioning pulse was necessary to inactivate the low-voltage-activating outward currents as shown previously (Ritter et al., 2012). The prepulse steady-state inactivation protocol consisted

Table 1. Properties of endogenous and recombinant Kv3.4 currents expressed in rat DRG neurons

Property	GFP	Kv3.4-WT	Kv3.4-PN	Kv3.4-PM	Kv3.4-DN
I_P (pA)[a]	65.70 ± 12.33	228.49 ± 47.06	224.44 ± 44.98	224.11 ± 67.82	2.01 ± 1.36
	$n = 16$	$n = 16$	$n = 35$	$n = 24$	$n = 13$
I_S (pA) at 500 ms[a]	17.40 ± 2.75	34.79 ± 8.68	7.29 ± 3.22	99.46 ± 25.65	0.27 ± 0.42
	$n = 16$	$n = 16$	$n = 32$	$n = 24$	$n = 11$
I_S /I_P	0.35 ± 0.05	0.21 ± 0.05	0.07 ± 0.04	1.11 ± 0.36	0.03 ± 0.24
	$n = 16$	$n = 16$	$n = 35$	$n = 24$	$n = 11$
Tau inactivation[a] (ms)	75.42 ± 22.87	33.18 ± 7.62	23.81 ± 4.21	115.06 ± 28.97	
	$n = 16$	$n = 16$	$n = 32$	$n = 24$	
Activation $V_{0.5}$ (mV)	27.40 ± 7.44	34.33 ± 4.38	25.29 ± 2.56	28.85 ± 3.68	
	$n = 16$	$n = 16$	$n = 35$	$n = 24$	
Activation z (e_0)	1.32 ± 0.19	0.82 ± 0.09	1.13 ± 0.10	1.19 ± 0.19	
	$n = 16$	$n = 16$	$n = 35$	$n = 24$	
Inactivation $V_{0.5}$ (mV)	−26.65 ± 4.77	−23.54 ± 3.57	−25.67 ± 1.85	3.86 ± 8.87	
	$n = 6$	$n = 5$	$n = 6$	$n = 5$	
Inactivation z (e_0)	1.56 ± 0.28	2.49 ± 0.14	2.55 ± 0.08	1.42 ± 0.3	
	$n = 6$	$n = 5$	$n = 6$	$n = 5$	

All values indicate mean ± SEM. Statistical analyses to evaluate differences are reported in Figures 3 and 4. I_P, Peak current; I_S, sustained current.
[a]At +100 mV.

of a varying 20 s conditioning pulse from −120 mV to +80 mV followed by a 300 ms test pulse to +80 mV.

Action potential experiments were performed as previously reported (Ritter et al., 2012, 2015b; Zemel et al., 2017). In these experiments, the external solution consisted of the following (in mM): 130 NaCl, 5 KCl, 2 $CaCl_2$, 1 $MgCl_2$, and 10 HEPES, whereas the internal solution consisted of 130 K-MES, 1 CaCl2, 1 EGTA, 10 HEPES, 2 Mg-ATP, and 0.3 Tris-GTP. Liquid junction potential (+15.5 mV for DRG recordings) was calculated using Clampex version 10.5 software, and voltages were corrected off-line.

Data analysis. Data processing and analysis were conducted in Clampfit 10.5 (Molecular Devices), Origin Pro 9.1 (OriginLab), Prism 9.3.1 (GraphPad), and RStudio release 2020.09.0 (PBC). Peak chord conductance–voltage (G_{Peak}-V_m) curves were generated from the peak current–voltage relations according to the following equation:

$$G_{Peak} = I_{Peak}/(V_m - E_r),$$

where V_m is the membrane potential, and E_r is the reversal potential of the high-voltage-activating K^+ current (−90 mV), as done previously (Ritter et al., 2012). Activation parameters were obtained from individual G_{Peak}-V_m curves by unweighted fitting of a first-order Boltzmann function of the following form:

$$G_{Peak} = G_{Pmax}/\left[1 + exp\left((V_m - V_{1/2})/s\right)\right],$$

where G_{Pmax} is the maximum conductance, $V_{1/2}$ is the midpoint voltage of the curve, and s is the slope factor (Table 1). The equivalent gating charge of activation z was determined from the following equation:

$$z = RT/sF,$$

where RT/F = 25.5 mV (R and F are standard physical abbreviations, and T = 296° K). For comparisons between individual recordings and different groups, the G_{Peak}-V_m curves were normalized with respect to the G_{Pmax} (G_{Peak}/G_{Pmax}) and plotted together. As done previously (Ritter et al., 2012), the prepulse inactivation parameters were determined from the unweighted best-fit first-order Boltzmann function of the following form:

$$I_{Peak} = \left(I_{Pmax}/\left[1 + exp(V_{1/2} - V_m)/s\right]\right) + C,$$

where I_{Pmax} is the maximum current, $V_{1/2}$ is the midpoint voltage of the curve, s is the slope factor, and C is a constant (Table 1). The equivalent gating charge of inactivation z was calculated as described above. For comparison between individual recordings and different groups, the prepulse inactivation curves were normalized with respect to the I_{Pmax} (I_{Peak}/I_{Pmax}) and plotted together. Time constants of macroscopic inactivation were determined from the best-fit sum of exponentials to the decay of the currents evoked by a step depolarization to +100 mV. As, especially at high voltages, the current decays are not exponential, we assumed a sum of exponential terms (generally two terms) and calculated the weighted time constant (Tau_w) according to the following equations:

$$I(t) = A_1 \exp(-t/Tau_1) + A_2 \exp(-t/Tau_2)$$

$$Tau_w = Tau_1[A_1/(A_1 + A_2)] + Tau_2[A_2/(A_1 + A_2)],$$

where A_1 and A_2 are the amplitudes of the terms. Passive and active membrane properties were determined as reported previously (Ritter et al., 2012; Zemel et al., 2017; Muqeem et al., 2018). Phase-plane plots were used to determine AP threshold (where the plot initially deviates from 0 mV/ms) and the maximum rates of depolarization and repolarization. The AP amplitude was measured as the difference between the peak overshoot and the lowest point of the afterhyperpolarization. The AP widths at 50% and 90% of the AP amplitude (APD_{50} and APD_{90}) were measured as previously described (Ritter et al., 2012).

Experimental design and statistical analysis. To facilitate data collection, no more than two experimental groups were generally included in each recording session, which typically took place over a period of 24–48 h. Reflecting heterogeneity, data at the necessary power were generally not normally distributed, and, therefore, the nonparametric Kruskal–Wallis one-way ANOVA test was used to evaluate the overall differences between the groups. Individual Mann–Whitney comparisons were then performed across groups with an appropriately adjusted alpha based on multiple comparisons. When appropriate and unless stated otherwise, summary measurements are presented as mean ± SEM (Table 1).

Results

Manipulations of Kv3.4 expression and current inactivation profile in DRG neurons

Previous work suggested that the expression, function, and modulation of Kv3.4 inactivation by PKC determines the repolarization of the AP in rat DRG neurons (Ritter et al., 2012; Zemel et al., 2018). However, a causal link was yet to be established. To directly manipulate Kv3.4 expression, function, and modulation in DRG neurons and establish the missing link, we created various AAV6 vectors encoding GFP only (transduction control),

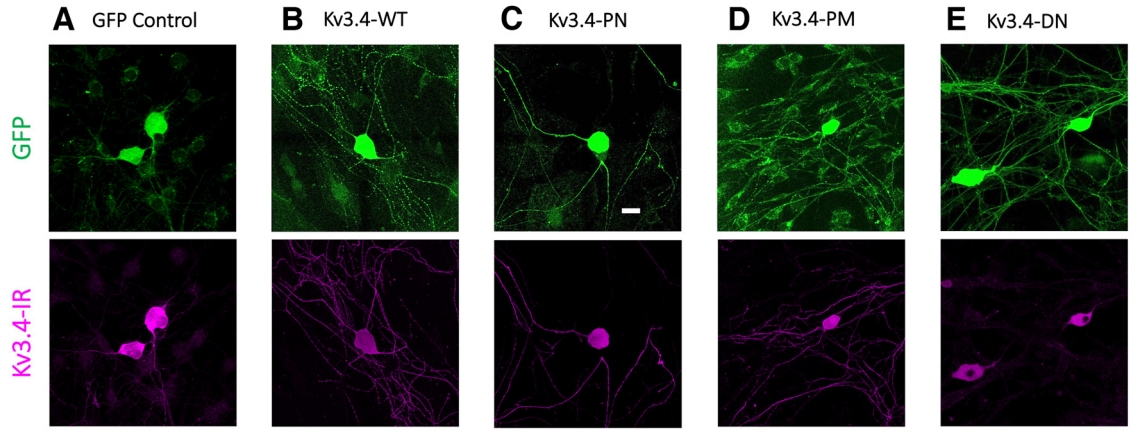

Figure 1. rAAV6 transduction of embryonic DRG neurons. ***A***, Fluorescence images of control DRG neurons infected with rAAV6 encoding GFP only. Six days after infection, the images demonstrate successful transduction and expression of the control GFP construct and endogenous Kv3.4 immunoreactivity (Kv3.4-IR). ***B–E***, Fluorescence images of DRG neurons infected with rAAV6 encoding GFP and the following recombinant Kv3.4 constructs indicated on the images: Kv3.4-WT, Kv3.4-PN, Kv3.4-PM and Kv3.4-DN. At 6 d postinfection, these images demonstrate robust transduction and colocalization of GFP fluorescence and Kv3.4-IR. Scale bar in ***C***, 20 μm for images in all panels..

wild-type (WT) Kv3.4, PN Kv3.4, PM Kv3.4, and DN Kv3.4 (see above, Materials and Methods). Whereas the endogenous Kv3.4 (in the GFP control) and the recombinant WT Kv3.4 have all NTID PKC sites available (S8, S9, S15, and S21), the Kv3.4-PN has none (S[8,9,15,21]A), and the Kv3.4-PM has all four sites mutated to aspartate (S[8,9,15,21]D). The Kv3.4-PM recapitulates the inactivation properties of the fully phosphorylated Kv3.4 on activation of PKC (Beck et al., 1998). Therefore, we used the Kv3.4-PM as an effective proxy of Kv3.4 with a fully phosphorylated NTID and refer to the effective phosphorylation status of the Kv3.4 NTID throughout the article. All Kv3.4 constructs included GFP as a reporter of transduction and expression.

Five to seven days after AAV6 infection of the embryonic DRG neurons, we assessed the expression of the proteins by fluorescence microscopy (see above, Materials and Methods). The control neurons displayed robust GFP fluorescence and basal Kv3.4 immunofluorescence, which was evident throughout the somata and processes of the neurons (Fig. 1*A*). Demonstrating high transduction efficiency, a vast majority of AAV6-treated neurons in all groups were GFP positive (~90%). Also, neurons infected with viral vectors encoding recombinant Kv3.4 proteins displayed strong Kv3.4 immunofluorescence (Kv3.4-IR) that colocalized with GFP fluorescence in the somata and processes, indicating successful transduction (Fig. 1*B–E*). Surprisingly, however, the Kv3.4 immunofluorescence was limited to the somata of neurons expressing the dominant-negative Kv3.4 mutant in three independent experiments. Qualitatively, we observed no correlation among GFP fluorescence, Kv3.4-IR, and functional expression.

To assess functional surface expression and characterize the resulting ionic currents, we recorded the macroscopic outward currents evoked by step depolarizations in the somatic cell-attached configuration of the patch-clamp method (see above, Materials and Methods). To isolate the high-voltage-activating K^+ currents, test pulses were preceded by a 1 s conditioning pulse to −50 mV (Ritter et al., 2012; Zemel et al., 2017), which inactivates most of the low-voltage-activating K^+ currents. Except for the neurons expressing the Kv3.4-DN mutant, in which we observed negligible currents, neurons in the remaining groups displayed outward currents exhibiting diverse transient and sustained components (Fig. 2). The voltage-dependent activation properties of these currents were, however, similar and consistent with the expression of high-voltage-activating Kv3.4 channels (Fig. 3*A–C*). The fluorescence microscopy and electrophysiological results demonstrate successful transduction and expression of recombinant Kv3.4 subunits, which may have formed both homotetrameric complexes and heterotetrameric complexes including the endogenous Kv3.4 subunit in DRG neurons. In particular, the robust knockdown effect of the Kv3.4-DN mutant demonstrates effective heterotetramerization of endogenous and recombinant Kv3.4 subunits.

The expression and effective phosphorylation status of Kv3.4 determine the profile of the outward currents in DRG neurons

To quantitatively characterize the profile of the evoked currents, we measured the following parameters at +100 mV, the voltage that evokes maximal activation of the conductance (Fig. 4): (1) peak current (I_P), (2) sustained current at the end of the depolarizing step (I_S), (3) the degree of inactivation as determined by the ratio of sustained current/peak current (I_S/I_P), and (4) the time constant of current decay (see above, Materials and Methods; Table 1, Fig. 4, including statistical analyses). The GFP only controls expressed relatively small endogenous outward currents (I_P = 65.7 ± 12.3 pA) displaying significant but incomplete inactivation (I_S/I_P = 0.35 ± 0.05) and a relatively slow time constant of inactivation (Tau = 75.4 ± 22.9 ms). Neurons that expressed recombinant Kv3.4-WT, Kv3.4-PN, and Kv3.4-PM subunits displayed larger outward currents that were on average similar in magnitude (228.5 ± 47.0 pA, 224.4 ± 45.0 pA, and 224.1 ± 67.8 pA, respectively) but different with respect to the degree of inactivation (0.21 ± 0.05, 0.07 ± 0.04, and 1.11 ± 0.36, respectively) and the time constant of inactivation at +100 mV (33.2 ± 7.6 ms, 23.8 ± 4.2 ms, and 115.1 ± 30 ms, respectively). Relative to the endogenous Kv3.4, these data show functional overexpression of the recombinant Kv3.4 subunits. Also, consistent with the effective expression of recombinant Kv3.4 subunits in DRG neurons, Kv3.4-DN induced a functional knockout of all high voltage-activating outward currents (Fig. 4. Table 1). It is, however, more significant that the expression of the Kv3.4-PN subunit conferred outward currents with the most profound inactivation (I_S/I_P of these currents is five and three times smaller than the corresponding values from GFP only controls and those from neurons expressing Kv3.4-WT, respectively). Also, the Kv3.4-PN subunit also conferred the fastest time constant of inactivation (~70 and 30% shorter than time constants from

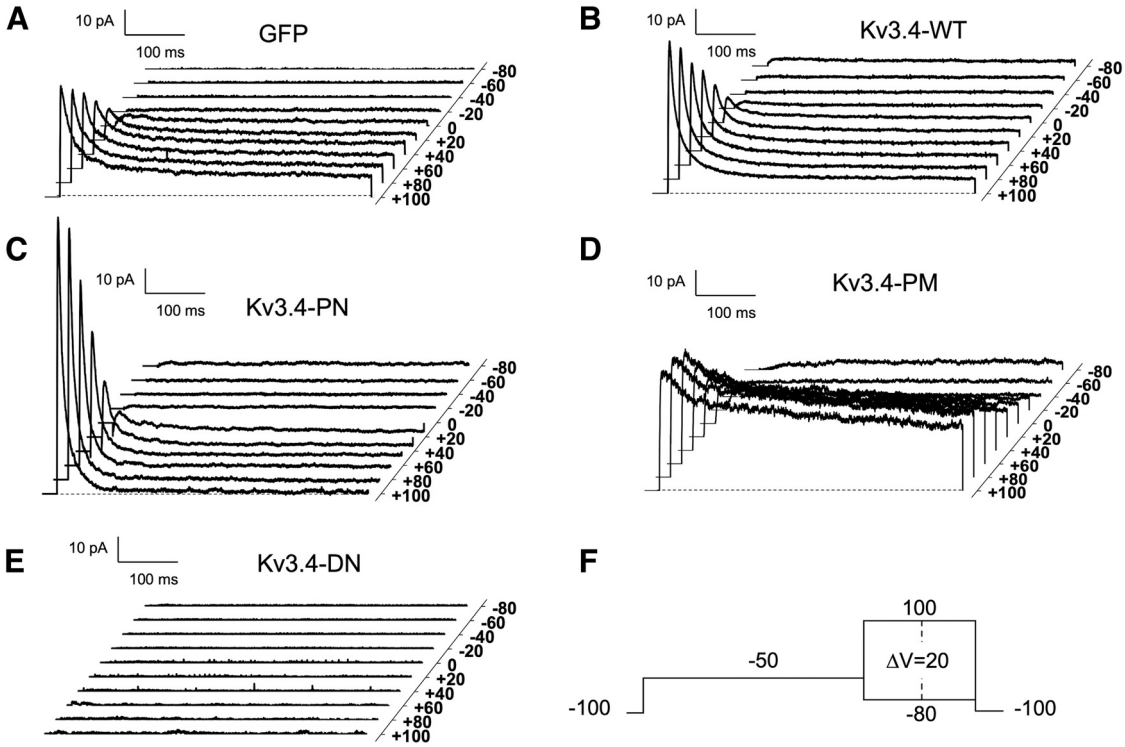

Figure 2. Functional expression of recombinant Kv3.4 subunits in cultured embryonic DRG neurons. ***A–E***, Representative families of cell-attached outward currents evoked by the pulse protocol shown on ***F***. A 1 s conditioning pulse is followed by a 500 ms test pulse. Whereas the control DRG neurons expressing GFP only display the endogenous Kv3.4 currents, DRG neurons coexpressing GFP and the indicated recombinant Kv3.4 channels display distinct current profiles.

GFP-only controls and neurons expressing Kv3.4-WT, respectively). Meanwhile, the Kv3.4-PM subunit conferred the opposite phenotype, the largest sustained current (~16 times larger than I_S/I_P, compared with the value from neurons expressing Kv3.4-PN) is accompanied by the slowest time constant of inactivation (~5-times slower than the time constant from neurons expressing Kv3.4-PN). These differences are particularly relevant because the Kv3.4-PN subunit would form Kv3.4 complexes resistant to phosphorylation, whereas complexes including Kv3.4-PM subunits are effectively fully phosphorylated. Consequently, complexes including Kv3.4-PM subunits exhibit the greatest destabilization of the inactivated state, which causes a substantial depolarizing shift in the prepulse inactivation curve (Fig. 3*D*,*F*). Analysis of this curve, however, does not offer sufficient resolution to detect possible changes induced by the other constructs. Nevertheless, considering the large difference between the current phenotypes induced by Kv3.4-PN and Kv3.4-PM subunits, it is also notable that Kv3.4-WT complexes bearing all PKC sites (endogenous and heterotetrameric) induced intermediate current profiles reflecting the intermediate extent of basal NTID phosphorylation, which may depend on the basal capacity of PKC to phosphorylate the endogenous homotetramers and heterotetramers including the overexpressed recombinant WT subunits. Reflecting the effective phosphorylation status of the Kv3.4 NTID at multiple sites in tetrameric complexes expressed in DRG neurons and differential cooperative effects on the binding and unbinding of the NTID to its receptor (Beck et al., 1998), a plot of the time constants of inactivation against the corresponding degree of inactivation revealed a positive nonlinear correlation (Fig. 4*F*). Thus, Kv3.4 inactivation is tunable in a manner that depends on the phosphorylation status of its NTID.

The expression and effective phosphorylation status of Kv3.4 dictate the maximum repolarization rate and width of the AP in DRG neurons

To determine the physiological impact of tunable Kv3.4 inactivation that depends on the phosphorylation of the Kv3.4 NTID, we characterized the AP waveform of DRG neurons expressing Kv3.4 subunits that differ in their effective NTID phosphorylation status under whole-cell current-clamping conditions (see above, Materials and Methods; Figs. 5, 6). The AP trajectories were qualitatively similar among all groups, characteristically displaying a maximal rate of depolarization (MRD) as the AP approaches its peak and a biphasic change in the rate of repolarization clearly evident in phase plane plots (Fig. 5, insets). Quantitatively, however, the AP_{peak} was modestly decreased in the groups of DRG neurons that expressed recombinant Kv3.4 subunits capable of forming functional complexes (Fig. 6*A*). The AP amplitude (AP_{peak} − AHP) displayed the same pattern, which was consistent with no significant change in the AHP (Fig. 6*B*, Table 2). In contrast, the 50% width of the APs (APD_{50}) changed mainly because of changes in the maximum rate of repolarization (MRR, Fig. 6). Whereas the Kv3.4-PM subunit conferred the shortest AP width (APD_{50} = 3.01 ± 0.17 ms), the Kv3.4-DN subunit conferred the longest AP widths, (APD_{50} = 5.62 ± 0.46 ms). Correspondingly, DRG neurons expressing the Kv3.4-PM subunit exhibited the fastest MRR (49.81 ± 2.27 = mV/ms), and those expressing the Kv3.4-DN subunit exhibited the slowest MRR (24.38 ± 1.79 mV/ms). It is also significant that the expression of the Kv3.4-PN conferred AP widths (APD_{50} = 4.14 ± 0.38 ms) that are intermediate between the values observed with DRG neurons expressing the Kv3.4-DN and the Kv3.4-PM subunits; and, accordingly, the corresponding APs also had an intermediate MRR (38.27 ± 3.78, mV/ms). The

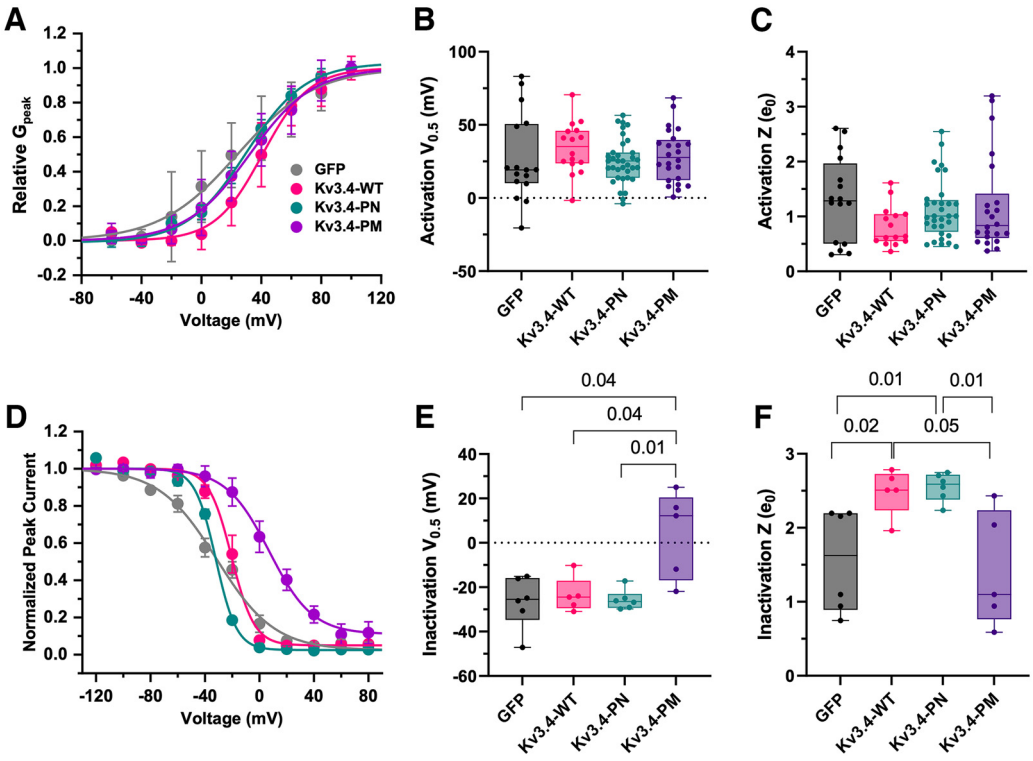

Figure 3. Voltage-dependent properties of cell-attached macroscopic currents induced by the overexpression of Kv3.4-WT, Kv3.4-PN, and Kv3.4-PM in embryonic DRG neurons. ***A***, Normalized peak conductance - voltage relations of endogenous and overexpressed Kv3.4 channels. The voltage protocol used to generate these relations is shown in Figure 2*F*. The solid lines are the best-fit first-order Boltzmann functions (see above, Materials and Methods). Best-fit parameters and shown in Table 1. ***B***, Scatter and box plots of the activation $V_{0.5}$. ***C***, Scatter and box plots of the activation equivalent gating charge. ***D***, Prepulse inactivation curves of endogenous and overexpressed Kv3.4 channels. The prepulse steady-state inactivation protocol consisted of a varying 20 s conditioning pulse from −120 mV to +80 mV followed by a 300 ms test pulse to +80 mV. The solid lines are the best-fit first-order Boltzmann functions (see above, Materials and Methods). Best-fit parameters are shown in Table 1. ***E***, Scatter and box plots of the inactivation $V_{0.5}$. ***F***, Scatter and box plots of the inactivation equivalent gating charge. The upper and lower borders of the boxes indicate the 75th and 25th percentiles, respectively; the line across the box indicates the 50th percentile, and the top and bottom whiskers indicate the maximum and minimum, respectively.

control GFP-only neurons and those expressing the Kv3.4-WT subunits exhibited AP widths and MRRs that were also intermediate, albeit generally closer to the values from neurons expressing the Kv3.4-PM subunit. These phenotypes may reflect variable basal PKC-dependent phosphorylation of still-available multiple NTID sites in tetrameric Kv3.4-WT channels.

Variations in the physiological properties of individual neurons, such as the resting membrane potential (RMP), may change the availability of voltage-gated Na^+ and K^+ channels and thereby affect the MRD and MRR of the AP, respectively (Fig. 6*F*). Therefore, the AP width would generally be a function of both the MRD and MRR. Accordingly, APs from neurons in the control GFP group exhibit significant negative correlations between APD_{50} and MRD and between APD_{50} and MRR (R^2 = 0.64, $p < 0.0001$ and R^2 = 0.88, $p < 0.0001$, respectively; Fig. 7*A*, *B*). However, when the DRG neurons overexpress the recombinant Kv3.4 subunits, we found stronger negative correlations between APD_{50} and MRR (R^2 = 0.49, $p < 0.0001$) than between APD_{50} and MRD (R^2 = 0.17, $p < 0.0001$; Fig. 7*C*,*D*). This difference was even more striking when we applied regression analysis to the mean values of each group (Fig. 7*E*,*F*). Whereas the correlation between APD_{50} and MRR is robust (R^2 = 0.99, p = 0.01), there is no correlation between APD_{50} and MRD (R^2 = 0.003, p = 0.95). Thus, the slowest MRRs and longest AP widths are associated with Kv3.4-DN expression, and the fastest MRRs and shortest AP widths are associated with Kv3.4-PM expression, whereas the intermediate MRRs and AP widths are associated with the expression in the remaining groups (Kv3.4-WT and Kv3.4-PN; Fig. 7*F*). As basal PKC activity is likely, correlation data from Kv3.4-WT (susceptible to NTID phosphorylation) and Kv3.4-PM (constitutively phosphorylated) are similar. This is in contrast to Kv3.4-PN, which cannot undergo NTID phosphorylation. Therefore, the neurons in the Kv3.4-PN group exhibit slower MRRs and longer AP widths (Fig. 7*F*). These results show that depending on its expression and effective phosphorylation status, Kv3.4 has a tunable ability to preferentially modulate the MRR and thereby determine AP width. Among all groups, by contrast, we observed no significant differences in RMP, input resistance (R_{in}), membrane capacitance (C_m), rheobase, and AP threshold ($p \geq 0.09$; Table 2). The absence of changes in RMP, R_{in}, and AP threshold is consistent with no effect of the NTID mutations on the characteristic high voltage activation of Kv3.4 (Fig. 3*A*–*C*).

Discussion

Previous work has demonstrated that Kv3.4 channels are significantly responsible for the active repolarization of the AP in DRG neurons and other neurons of the CNS (Ritter et al., 2012; Rowan et al., 2016; Liu et al., 2017; Rowan and Christie, 2017). Particularly, our work suggests that this role depends on the phosphorylation status of the Kv3.4 NTID (Covarrubias et al., 1994; Beck et al., 1998; Ritter et al., 2012). However, a causal link between NTID phosphorylation, Kv3.4 inactivation kinetics, and the properties of the AP was lacking. Here, we manipulated Kv3.4 expression and the effective phosphorylation status of Kv3.4

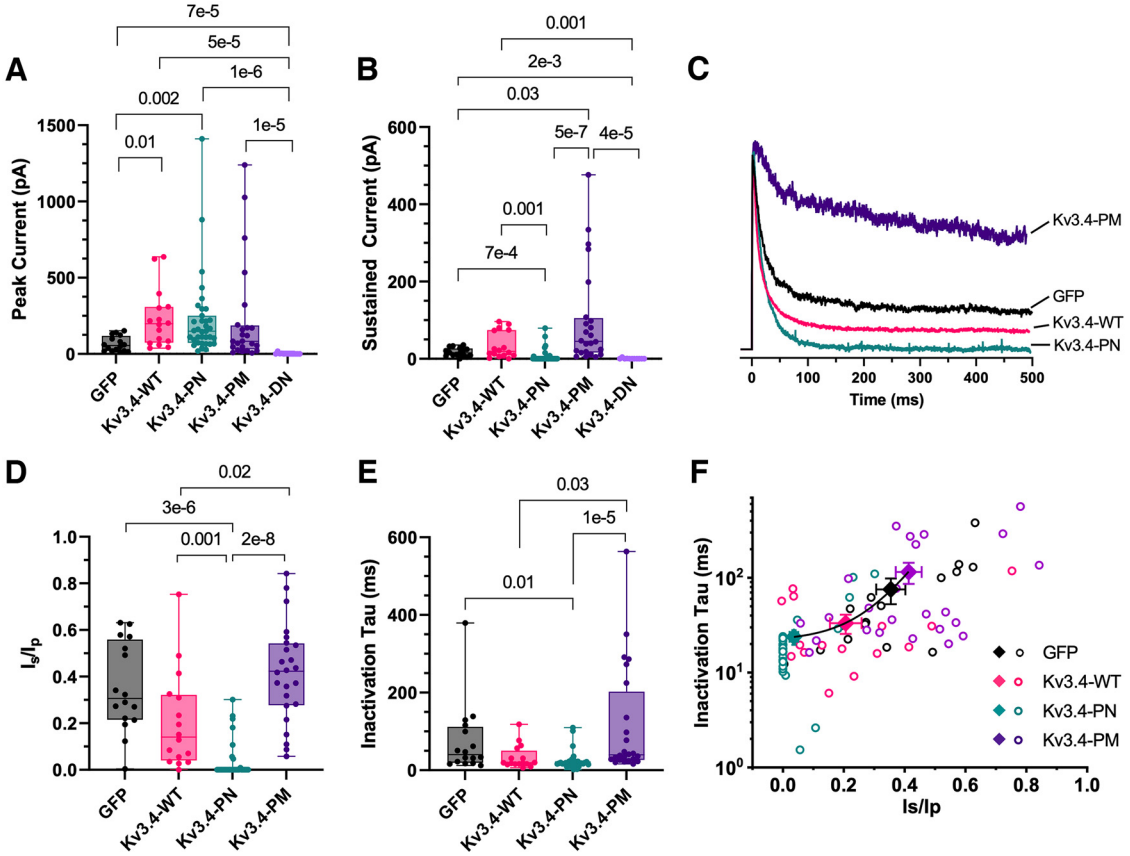

Figure 4. Kinetic properties of cell-attached macroscopic currents induced by the overexpression of Kv3.4-WT, Kv3.4-PN, Kv3.4-PM, and Kv3.4-DN in embryonic DRG neurons. ***A***, ***B***, Scatter and box plots of the peak and sustained currents evoked by the pulse protocol shown on Fig. 2*F*. ***C***, Overlay of representative scaled macroscopic currents evoked by the pulse protocol shown on Fig. 2*F*. ***D***, ***E***, Scatter and box plots of the ratio of sustained current over peak current (*Is*/*Ip*) and the time constant of macroscopic inactivation at +100 mV. The features of the box plots are as described in Figure 3. ***F***, Correlation between the inactivation time constant and the *Is*/*Ip*. Filled diamonds and crossbars represent the mean values with their corresponding SEM. Hollow symbols represent the independent measurements from individual neurons in the color-coded groups indicated by the legend of the graph (right). The correlation is empirically described by the following exponential equation (solid line): $y = 1.49[\exp(x/0.1)]$.

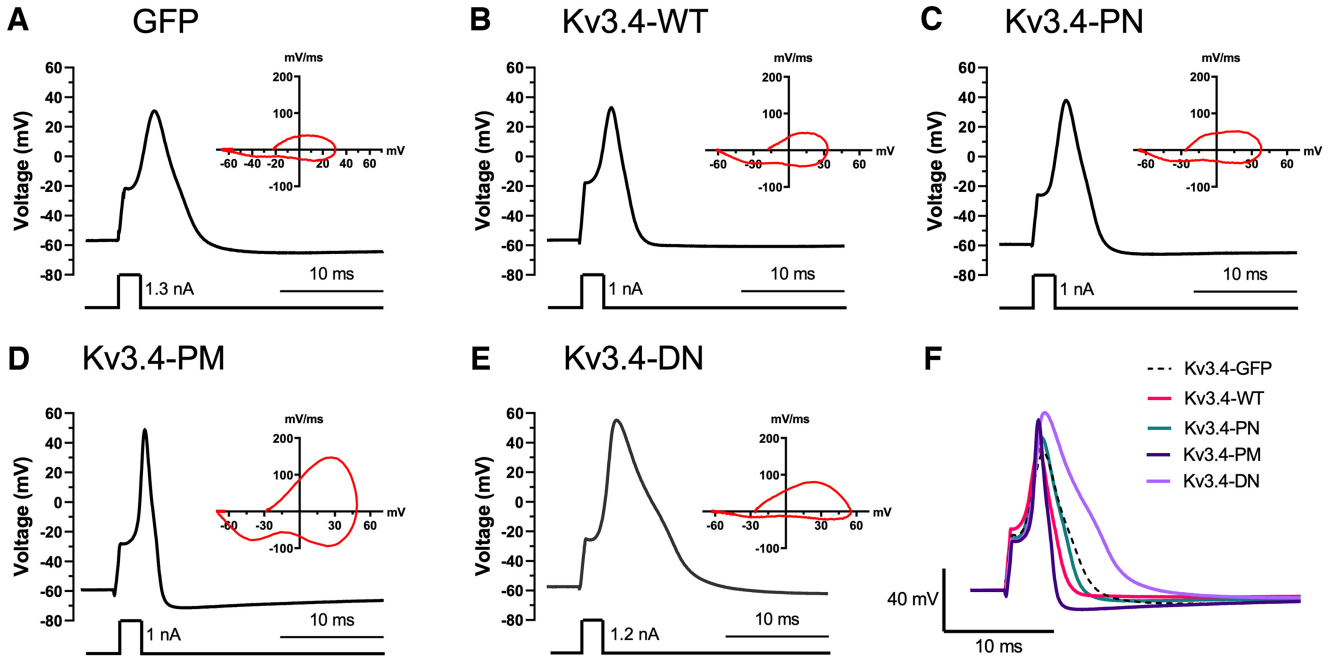

Figure 5. Action potential trajectories following manipulations of the expression and effective phosphorylation status of Kv3.4 in DRG neurons. ***A–E***, Representative AP waveforms evoked by the indicated 0.5 ms current injection pulse. Insets, Corresponding phase plane plot for each group. ***F***, Overlay of representative AP waveforms from the indicated color-coded groups. The RMPs for Kv3.4-GFP, WT, PN, PM, and DN were −56.8, −56.6, −59.2, −59.2, and −57.4 mV, respectively. For direct comparison of the AP trajectories, the RMPs of the overlaid traces are normalized.

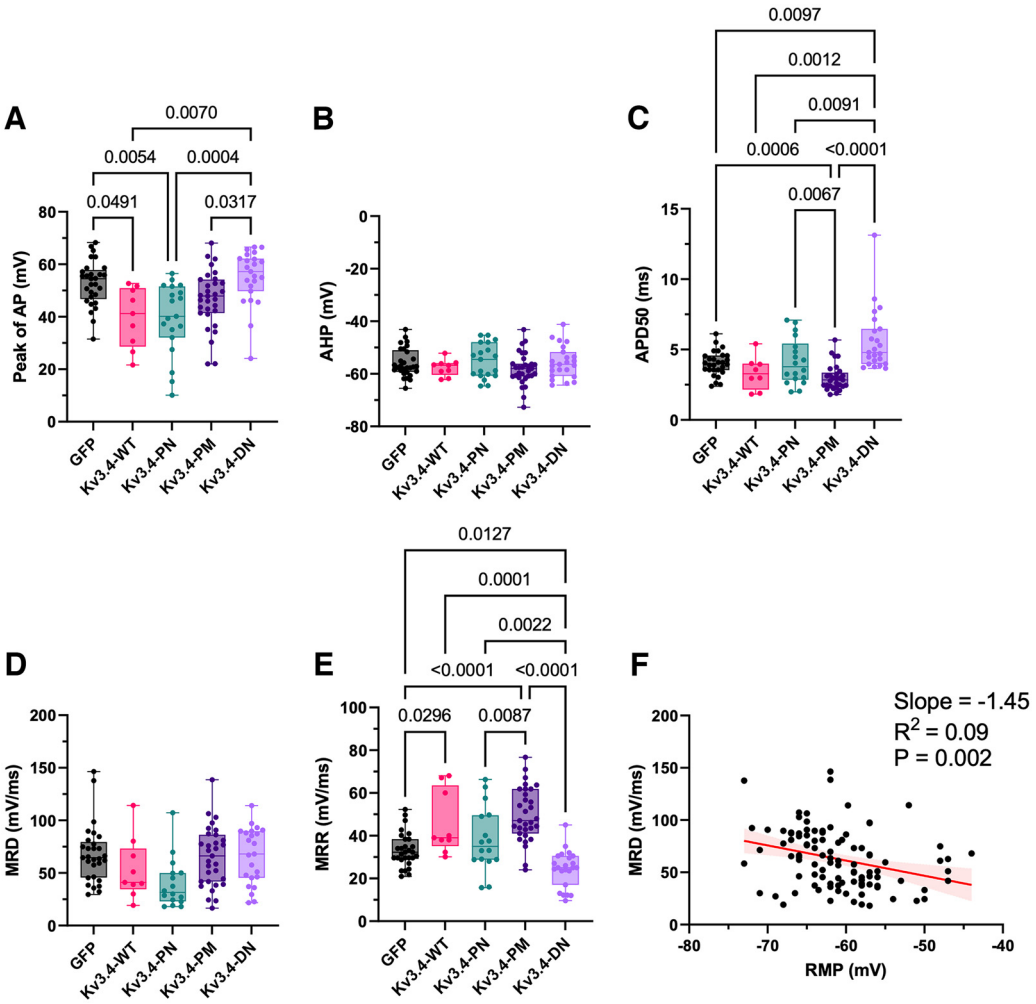

Figure 6. Action potential properties following manipulations of the expression and effective phosphorylation status of Kv3.4 in DRG neurons. ***A–E***, Scatter and box plots of the AP peak amplitude, AHP, APD_{50}, MRD, and MRR, as indicated by the *y*-axis of the graph. The features of the box plots are as described in Figure 3. ***F***, Correlation between MRD and RMP. The red solid line is the best-fit linear regression with the parameters (slope, R^2 and *P*) indicated on the graph, and the shaded area represents the confidence limits of the regression. A similar weak correlation was found between MRR and RMP (slope = −0.13, $R^2 = 0.10$, and $p = 0.0007$).

Table 2. Passive and active membrane properties of DRG neurons upon manipulations of Kv3.4 expression and effective phosphorylation status

Property	GFP Control	Kv3.4-WT	Kv3.4-PN	Kv3.4-PM	Kv3.4-DN
RMP (mV)	−62.14 ± 1.21	−59.63 ± 1.64	−60.50 ± 1.34	−61.48 ± 1.08	−59.66 ± 1.28
	n = 29	*n* = 9	*n* = 19	*n* = 31	*n* = 23
Ri (GΩ)	0.44 ± 0.05	0.37 ± 0.06	0.33 ± 0.06	0.46 ± 0.05	0.38 ± 0.05
	n = 29	*n* = 8	*n* = 15	*n* = 29	*n* = 21
Cm (pF)	20.84 ± 1.33	20.51 ± 3.82	15.33 ± 2.02	23.48 ± 1.53	19.79 ± 1.25
	n = 29	*n* = 9	*n* = 19	*n* = 31	*n* = 23
Rheobase (pA)	121.21 ± 15.13	106.25 ± 18.80	111.18 ± 12.00	142.62 ± 17.70	165.81 ± 31.35
	n = 28	*n* = 8	*n* = 17	*n* = 29	*n* = 21
AP threshold (mV)	−20.55 ± 1.2	−16.00 ± 2.4	−16.47 ± 1.2	−18.71 ± 1.4	−16.85 ± 1.5
	n = 29	*n* = 9	*n* = 19	*n* = 31	*n* = 13
AP peak (mV)	52.79 ± 1.59	39.73 ± 3.83	39.40 ± 3.12	46.80 ± 1.95	55.11 ± 2.16
	n = 29	*n* = 9	*n* = 19	*n* = 31	*n* = 23
AHP (mV)	−55.82 ± 1.00	−57.68 ± 1.04	−55.17 ± 1.50	−58.12 ± 1.09	−55.57 ± 1.27
	n = 29	*n* = 9	*n* = 19	*n* = 31	*n* = 23
AP amplitude (mV)	108.61 ± 1.57	97.41 ± 3.90	94.57 ± 3.61	104.92 ± 2.25	110.68 ± 2.95
	n = 29	*n* = 9	*n* = 19	*n* = 31	*n* = 23
MRD (mV/ms)	67.89 ± 5.09	53.43 ± 9.75	40.00 ± 5.92	65.25 ± 5.06	66.27 ± 5.58
	n = 29	*n* = 9	*n* = 16	*n* = 31	*n* = 23
MRR (mV/ms)	33.28 ± 1.48	45.83 ± 4.97	38.27 ± 3.78	49.81 ± 2.27	24.38 ± 1.79
	n = 29	*n* = 9	*n* = 16	*n* = 31	*n* = 23

All values are mean ± SEM. Statistical analyses to evaluate differences are reported in Figure 6. Among all groups, RMP, R_i, C_m, rheobase, and AP threshold were not significantly different ($p \geq 0.09$).

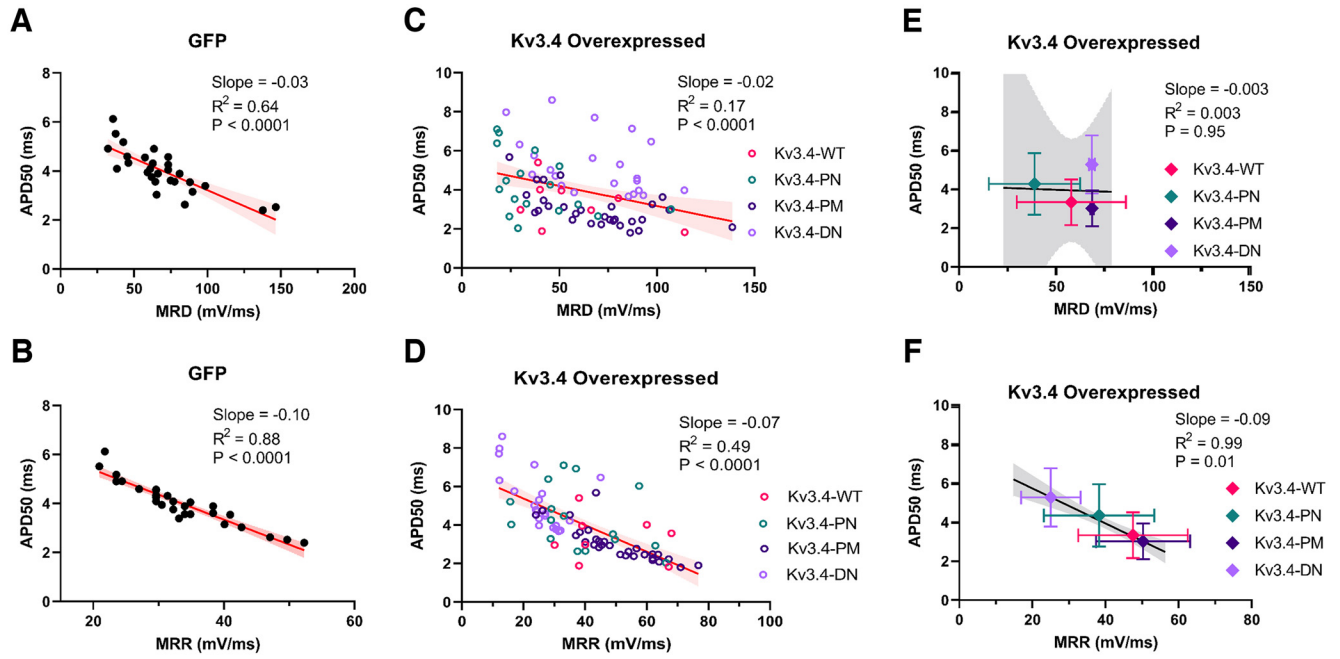

Figure 7. Correlations between action potential properties under conditions that manipulate Kv3.4 expression and effective phosphorylation status in DRG neurons. ***A***, ***B***, Correlations between APD_{50} and MRD, and between APD_{50} and MRR, respectively, from the control GFP group only. ***C***, ***D***, Global correlations of APD_{50} versus MRD and APD_{50} versus MRR, respectively, from all groups overexpressing Kv3.4 subunits (Kv3.4-WT, Kv3.4-PN, Kv3.4-PM, and Kv3.4-DN). In all graphs, the solid lines are the best-fit linear regressions with the parameters (slope, R^2 and *P*) indicated on each graph. The shaded areas represent the confidence limits of the regressions. ***E***, ***F***, Correlations of mean APD50 versus mean MRD and mean APD50 versus mean MRR, respectively.

heteromultimers (composed of endogenous and recombinant subunits) in DRG neurons to directly demonstrate predictable changes in the profile of macroscopic Kv3.4 inactivation and the resulting changes in the properties of the AP waveform. We propose that this mechanism underlies AP plasticity and diversity in DRG neurons and other central neurons that express Kv3.4 subunits.

The mechanism of tunable regulation of AP repolarization by Kv3.4 channels

PKC-dependent phosphorylation of the Kv3.4 NTID at four nonequivalent sites induces a conformational change in the NTID from structured to disordered, which is responsible for elimination of fast N-type inactivation in Kv3.4 channels (Beck et al., 1998; Antz et al., 1999). Also, activation of PKC with phorbol esters in DRG neurons slows inactivation of Kv3.4 channels, shortens the AP, and accelerates the maximum rate of AP repolarization (Ritter et al., 2012). These AP changes are dependent on the expression of Kv3.4, albeit, additionally associated with unexpected shifts (i.e., the maximum rate of AP depolarization), and we could not rule out that chemical PKC activation affects the AP by modulating additional ion channels and indirect effects from other PKC-dependent signaling networks (Li et al., 1993; Levitan, 1994; Cantrell et al., 2002; Levitan, 2006; Dai et al., 2009). The results reported here overcome this uncertainty in rat DRG neurons by directly demonstrating that (1) the Kv3.4-DN mutant induces a robust knockdown of the Kv3.4 current that is associated with AP broadening and decreased MRR without significantly altering the MRD, (2) the Kv3.4-PM mutant induces currents with impaired inactivation that is associated with AP shortening and increased MRR without significantly altering the MRD, (3) the Kv3.4-PN mutant induces currents with fast and profound inactivation that is associated with AP properties that are intermediate between those of DRG neurons expressing the Kv3.4-DN and Kv3.4-PM, and (4) the endogenous Kv3.4 currents and those induced by Kv3.4-WT overexpression exhibit hybrid inactivation properties associated with hybrid AP properties, which possibly reflect the availability of all four PKC sites at the NTID and basal PKC activity in DRG neurons (Zemel et al., 2017).

Following the specific manipulations of Kv3.4 effective phosphorylation status in DRG neurons, the analysis of current kinetics and voltage dependence of inactivation revealed the key role of inactivation modulation in the way Kv3.4 regulates the AP. The nonlinear relationship between the time constant of macroscopic inactivation and the fractional sustained current demonstrates that inactivation is gradually impaired between the phenotypes of the Kv3.4-PN and the Kv3.4-PM, whereas the Kv3.4-WT and the endogenous Kv3.4 have intermediate phenotypes (Fig. 3*F*). This is consistent with the reported nonlinear effects of NTID phosphorylation on the binding and unbinding rate constants controlling the interaction of the NTID with a putative pore receptor (Beck et al., 1998). It is also significant that the prepulse inactivation curve of heteromultimeric Kv3.4 channels including Kv3.4-PM subunits displays a substantial depolarizing shift resulting from destabilization of the inactivated state, as previously shown (Beck et al., 1998). The picture that emerges from these observations is one in which the availability of Kv3.4 channels and gradual changes in their inactivation properties are directly responsible for a tunable regulation of AP repolarization. Strengthening this conclusion, the APD_{50} and MRR are strongly correlated in a way that depends on Kv3.4 inactivation properties as determined by Kv3.4 expression and effective phosphorylation status. In contrast, there is only a weak correlation between the APD_{50} and MRD.

Signaling molecules and pathways that determine the phosphorylation status of the Kv3.4 NTID

Significant evidence has demonstrated the modulation of ion channels by PKCs in DRG neurons and the role and importance

of G-protein-coupled receptors (GPCR) in DRG neurons under physiological and pathologic conditions (Souza et al., 2002; Hucho and Levine, 2007). Following exposure of DRG neurons to a cocktail of GPCR agonists (histamine, serotonin, and bradykinin), we have previously shown elimination of Kv3.4 fast inactivation in a membrane-delimited fashion and shortening of AP duration, resembling the observations reported here (Ritter et al., 2012). Also, exposure to serotonin alone is sufficient to induce elimination of Kv3.4 inactivation following heterologous coexpression of Kv3.4 and the metabotropic serotonin receptor 1C (Velasco et al., 1998); and Ca^{++}-dependent PKC isoforms can phosphorylate the Kv3.4 NTID *in vitro* (Covarrubias et al., 1994). More recent studies have also shown that Kv3.4 undergoes PKC-dependent modulation of fast inactivation under basal conditions (absence of chemical and agonist activation of PKC), and suggest that calcineurin (CaN) is the phosphatase that dephosphorylates the Kv3.4 NTID (Zemel et al., 2017). Thus, under physiological conditions it seems that the balance between Ca^{++}-dependent PKCs and CaN maintains the phosphorylation status of the Kv3.4 NTID and, consequently, the inactivation properties of the ion channel. Therefore, in conjunction with the results reported here, we now have compelling evidence to conclude that the repolarization rate of the AP in DRG neurons is causally linked to the inactivation properties of the Kv3.4 channel as determined by the PKC-dependent phosphorylation status of the Kv3.4 NTID.

Neurophysiological implications in health and disease

Kv3 channels play a major role in the nervous system by regulating ultra-fast-spiking and evoked synaptic transmission (Rudy and McBain, 2001; Kaczmarek and Zhang, 2017; Zemel et al., 2018). This regulation depends on the specialized ability of Kv3 channels to quickly repolarize the AP and thereby shorten its width. Kv3.1 and Kv3.2 are particularly capable of playing this role in fast-spiking GABAergic interneurons because they are high-voltage-activating delayed rectifying Kv channels that undergo minimal slow inactivation on suprathreshold depolarizations of the membrane potential. In contrast, the dephosphorylated Kv3.4 is an A-type Kv channel that undergoes fast inactivation induced by subthreshold and suprathreshold membrane potential depolarizations and, therefore, has a limited ability to play this role. Frequency-dependent spike broadening in small-diameter DRG neurons may in part result from Kv3.4 inactivation (Liu et al., 2017). We propose that the Kv3.4 channel is a delayed rectifying Kv channel in disguise, which springs into action upon phosphorylation of its NTID to oppose frequency-dependent spike broadening. This action is, however, tunable, depending on both expression and phosphorylation status of the NTID. In instances where the phosphorylated Kv3.4 is part of a Kv3 heterotetramer, it would confer the ability to quickly repolarize the AP and promote fast spiking. In this case, the impact of Kv3.4 would also depend on the constitutive properties of specific Kv3.4 splice variants and the stoichiometry of the heterotetramer in particular neuronal subtypes and subcellular compartments (Baranauskas et al., 2003). Considering these factors, the contributions of Kv3.4 to neurophysiological properties would be variable and susceptible to complex regulation involving transcriptional, post-transcriptional (splicing), and post-translational (NTID phosphorylation) factors. Because Kv3.4 is also discretely expressed in the cerebrum, cerebellum, the neuromuscular junction, and skeletal muscle, we propose that this regulation may also play a major role shaping the AP in these tissues (Abbott et al., 2001; Rudy and McBain, 2001; Baranauskas et al., 2003; Martina et al., 2003; Brooke et al., 2004a, b; Rowan et al., 2016; Kaczmarek and Zhang, 2017; Ojala et al., 2021).

Although congenital disorders directly implicating KCNC4 (Kv3.4 gene) variants have not been reported, Kv3.4 anomalies have been found in neurologic diseases, including neuropathic pain and Alzheimer's disease (Pannaccione et al., 2007; Ritter et al., 2015a; Boscia et al., 2017; Zemel et al., 2017; Yeap et al., 2022). In spinal-cord-injury-induced neuropathic pain, NTID phosphorylation is dysregulated in DRG neurons, where we found upregulation of the endogenous CaN inhibitor RCAN1 (Zemel et al., 2017). As CaN is the phosphatase responsible for the dephosphorylation of the Kv3.4 NTID, CaN inhibition may lead to dysregulated NTID hyperphosphorylation. As a result, slow inactivating Kv3.4 currents in this pathologic scenario are inhibited by an unknown mechanism (Zemel et al., 2017, 2018). This inhibition is a factor that may contribute to the DRG neuron hyperexcitability associated the spinal-cord-injury-induced neuropathic pain (Ritter et al., 2015a, b).

Conclusion and perspective

We conclude that the inactivation properties of Kv3.4 channels in DRG neurons are directly dependent on the effective phosphorylation status of the Kv3.4 NTID and that this in turn underlies a tunable mechanism to modulate the rate of AP repolarization and, consequently, AP width. Generally, this mechanism would directly affect neurophysiological processes that depend on AP repolarization rate and duration such as evoked synaptic transmission and fast spiking in neurons where Kv3.4 is expressed as a homotetramer or is part of heterotetramers including other Kv3 subunits. The impact of this modulation at the circuit and behavioral levels is, however, unknown, and more work is needed to understand it *in vivo* under physiological and pathologic conditions.

References

Abbott GW, Butler MH, Bendahhou S, Dalakas MC, Ptacek LJ, Goldstein SA (2001) MiRP2 forms potassium channels in skeletal muscle with Kv3.4 and is associated with periodic paralysis. Cell 104:217–231.

Antz C, Bauer T, Kalbacher H, Frank R, Covarrubias M, Kalbitzer HR, Ruppersberg JP, Baukrowitz T, Fakler B (1999) Control of K+ channel gating by protein phosphorylation: structural switches of the inactivation gate. Nat Struct Biol 6:146–150.

Baranauskas G, Tkatch T, Nagata K, Yeh JZ, Surmeier DJ (2003) Kv3.4 subunits enhance the repolarizing efficiency of Kv3.1 channels in fast-spiking neurons. Nat Neurosci 6:258–266.

Bean BP (2007) The action potential in mammalian central neurons. Nat Rev Neurosci 8:451–465.

Beck EJ, Sorensen RG, Slater SJ, Covarrubias M (1998) Interactions between multiple phosphorylation sites in the inactivation particle of a K+ channel. Insights into the molecular mechanism of protein kinase C action. J Gen Physiol 112:71–84.

Boscia F, Pannaccione A, Ciccone R, Casamassa A, Franco C, Piccialli I, de Rosa V, Vinciguerra A, Di Renzo G, Annunziato L (2017) The expression and activity of KV3.4 channel subunits are precociously upregulated in astrocytes exposed to Aβ oligomers and in astrocytes of Alzheimer's disease Tg2576 mice. Neurobiol Aging 54:187–198.

Brooke RE, Atkinson L, Batten TF, Deuchars SA, Deuchars J (2004a) Association of potassium channel Kv3.4 subunits with pre- and post-synaptic structures in brainstem and spinal cord. Neuroscience 126:1001–1010.

Brooke RE, Moores TS, Morris NP, Parson SH, Deuchars J (2004b) Kv3 voltage-gated potassium channels regulate neurotransmitter release from mouse motor nerve terminals. Eur J Neurosci 20:3313–3321.

Cantrell AR, Tibbs VC, Yu FH, Murphy BJ, Sharp EM, Qu Y, Catterall WA, Scheuer T (2002) Molecular mechanism of convergent regulation of brain Na(+) channels by protein kinase C and protein kinase A anchored to AKAP-15. Mol Cell Neurosci 21:63–80.

Carter BC, Bean BP (2009) Sodium entry during action potentials of mammalian neurons: incomplete inactivation and reduced metabolic efficiency in fast-spiking neurons. Neuron 64:898–909.

Covarrubias M, Wei A, Salkoff L, Vyas TB (1994) Elimination of rapid potassium channel inactivation by phosphorylation of the inactivation gate. Neuron 13:1403–1412.

Dai S, Hall DD, Hell JW (2009) Supramolecular assemblies and localized regulation of voltage-gated ion channels. Physiol Rev 89:411–452.

Desai R, Kronengold J, Mei J, Forman SA, Kaczmarek LK (2008) Protein kinase C modulates inactivation of Kv3.3 channels. J Biol Chem 283:22283–22294.

Hochner B, Kandel ER (1992) Modulation of a transient K+ current in the pleural sensory neurons of Aplysia by serotonin and cAMP: implications for spike broadening. Proc Natl Acad Sci U S A 89:11476–11480.

Hucho T, Levine JD (2007) Signaling pathways in sensitization: toward a nociceptor cell biology. Neuron 55:365–376.

Kaczmarek LK, Zhang Y (2017) Kv3 Channels: enablers of rapid firing, neurotransmitter release, and neuronal endurance. Physiol Rev 97:1431–1468.

Kimm T, Khaliq ZM, Bean BP (2015) Differential regulation of action potential shape and burst-frequency firing by BK and Kv2 channels in substantia nigra dopaminergic neurons. J Neurosci 35:16404–16417.

Koch C (1999) Biophysics of computation: information processing in single neurons. New York: Oxford UP.

Levitan IB (1994) Modulation of ion channels by protein phosphorylation and dephosphorylation. Annu Rev Physiol 56:193–212.

Levitan IB (2006) Signaling protein complexes associated with neuronal ion channels. Nat Neurosci 9:305–310.

Li M, West JW, Numann R, Murphy BJ, Scheuer T, Catterall WA (1993) Convergent regulation of sodium channels by protein kinase C and cAMP-dependent protein kinase. Science 261:1439–1442.

Liu PW, Bean BP (2014) Kv2 channel regulation of action potential repolarization and firing patterns in superior cervical ganglion neurons and hippocampal CA1 pyramidal neurons. J Neurosci 34:4991–5002.

Liu PW, Blair NT, Bean BP (2017) Action potential broadening in capsaicin-sensitive DRG neurons from frequency-dependent reduction of Kv3 current. J Neurosci 37:9705–9714.

Ma M, Koester J (1996) The role of K+ currents in frequency-dependent spike broadening in Aplysia R20 neurons: a dynamic-clamp analysis. J Neurosci 16:4089–4101.

Martina M, Yao GL, Bean BP (2003) Properties and functional role of voltage-dependent potassium channels in dendrites of rat cerebellar Purkinje neurons. J Neurosci 23:5698–5707.

Mitterdorfer J, Bean BP (2002) Potassium currents during the action potential of hippocampal CA3 neurons. J Neurosci 22:10106–10115.

Muqeem T, Ghosh B, Pinto V, Lepore AC, Covarrubias M (2018) Regulation of nociceptive glutamatergic signaling by presynaptic Kv3.4 channels in the rat spinal dorsal horn. J Neurosci 38:3729–3740.

Ojala KS, Ginebaugh SP, Wu M, Miller EW, Ortiz G, Covarrubias M, Meriney SD (2021) A high-affinity, partial antagonist effect of 3,4-diaminopyridine mediates action potential broadening and enhancement of transmitter release at NMJs. J Biol Chem 296:100302.

Pannaccione A, Boscia F, Scorziello A, Adornetto A, Castaldo P, Sirabella R, Taglialatela M, Di Renzo GF, Annunziato L (2007) Up-regulation and increased activity of KV3.4 channels and their accessory subunit MinK-related peptide 2 induced by amyloid peptide are involved in apoptotic neuronal death. Mol Pharmacol 72:665–673.

Pathak D, Guan D, Foehring RC (2016) Roles of specific Kv channel types in repolarization of the action potential in genetically identified subclasses of pyramidal neurons in mouse neocortex. J Neurophysiol 115:2317–2329.

Quattrocki EA, Marshall J, Kaczmarek LK (1994) A Shab potassium channel contributes to action potential broadening in peptidergic neurons. Neuron 12:73–86.

Ritter DM, Ho C, O'Leary ME, Covarrubias M (2012) Modulation of Kv3.4 channel N-type inactivation by protein kinase C shapes the action potential in dorsal root ganglion neurons. J Physiol 590:145–161.

Ritter DM, Zemel BM, Hala TJ, O'Leary ME, Lepore AC, Covarrubias M (2015a) Dysregulation of Kv3.4 channels in dorsal root ganglia following spinal cord injury. J Neurosci 35:1260–1273.

Ritter DM, Zemel BM, Lepore AC, Covarrubias M (2015b) Kv3.4 channel function and dysfunction in nociceptors. Channels (Austin) 9:209–217.

Rowan MJ, Christie JM (2017) Rapid state-dependent alteration in Kv3 channel availability drives flexible synaptic signaling dependent on somatic subthreshold depolarization. Cell Rep 18:2018–2029.

Rowan MJ, Tranquil E, Christie JM (2014) Distinct Kv channel subtypes contribute to differences in spike signaling properties in the axon initial segment and presynaptic boutons of cerebellar interneurons. J Neurosci 34:6611–6623.

Rowan MJ, DelCanto G, Yu JJ, Kamasawa N, Christie JM (2016) Synapse-level determination of action potential duration by K(+) channel clustering in axons. Neuron 91:370–383.

Rudy B, McBain CJ (2001) Kv3 channels: voltage-gated K+ channels designed for high-frequency repetitive firing. Trends Neurosci 24:517–526.

Rudy B, Sen K, Vega-Saenz de Miera E, Lau D, Ried T, Ward DC (1991) Cloning of a human cDNA expressing a high voltage-activating, TEA-sensitive, type-A K+ channel which maps to chromosome 1 band p21. J Neurosci Res 29:401–412.

Schröter KH, Ruppersberg JP, Wunder F, Rettig J, Stocker M, Pongs O (1991) Cloning and functional expression of a TEA-sensitive A-type potassium channel from rat brain. FEBS Lett 278:211–216.

Souza AL, Moreira FA, Almeida KR, Bertollo CM, Costa KA, Coelho MM (2002) *In vivo* evidence for a role of protein kinase C in peripheral nociceptive processing. Br J Pharmacol 135:239–247.

Tymanskyj SR, Curran BM, Ma L (2022) Selective axonal transport through branch junctions is directed by growth cone signaling and mediated by KIF1/kinesin-3 motors. Cell Rep 39:110748.

Velasco I, Beck EJ, Covarrubias M (1998) Receptor-coupled regulation of K+ channel N-type inactivation. Neurobiology (Bp) 6:23–32.

Yeap J, Sathyaprakash C, Toombs J, Tulloch J, Scutariu C, Rose J, Burr K, Davies C, Colom-Cadena M, Chandran S, Large CH, Rowan MJM, Gunthorpe MJ, Spires-Jones TL (2022) Reducing voltage-dependent potassium channel Kv3.4 levels ameliorates synapse loss in a mouse model of Alzheimer's disease. Brain Neurosci Adv 6:23982128221086464.

Zemel BM, Muqeem T, Brown EV, Goulao M, Urban MW, Tymanskyj SR, Lepore AC, Covarrubias M (2017) Calcineurin dysregulation underlies spinal cord injury-induced K+ channel dysfunction in DRG neurons. J Neurosci 37:8256–8272.

Zemel BM, Ritter DM, Covarrubias M, Muqeem T (2018) A-type KV channels in dorsal root ganglion neurons: diversity, function, and dysfunction. Front Mol Neurosci 11:253.

Zheng Y, Liu P, Bai L, Trimmer JS, Bean BP, Ginty DD (2019) Deep sequencing of somatosensory neurons reveals molecular determinants of intrinsic physiological properties. Neuron 103:598–616.e7.